10th IMC
10th International Masonry Conference
G. Milani, A. Taliercio and S. Garrity (eds.)
Milan, Italy, July 9-11, 2018

MODELLING OF MASONRY ARCHES STRENGTHENED AT EXTRADOS WITH FRCM

Eleonora Ricci[1], Daniel V. Oliveira[2], Elio Sacco[3] and Bahman Ghiassi[4]

[1] University of Cassino and SL
via G. di Biasio, 43, Cassino, Italy
e-mail: e.ricci@unicas.it

[2] University of Minho
Campus de Azurém, Guimarães, Portugal
danvco@civil.uminho.pt

[3] University of Naples Federico II
Via Claudio, 21, Napoli, Italy
elio.sacco@unina.it

[4] Delft University of Technology
Mekelweg, 2, Delft, The Netherlands
b.ghiassi@tudelft.nl

Keywords: FRCM, Masonry, Arches, Numerical Analysis, Reinforcement.

Abstract. Masonry arches are amongst the most fascinating structures of the World's historical and architectural heritage. Their vulnerability to earthquakes pointed out the necessity of their preservation. Fiber Reinforced Cementitious Mortar (FRCM) composites have been recently used as a more sustainable alternative to FRPs in the strengthening of masonry structures, since they can overcome the limits FRP show as strengthening systems: poor behavior to high temperature, delamination with significant loss of material at the bonded surface, lack of vapor permeability, impossibility of application on humid surfaces, incompatibility of resins with masonry, high cost and reduced reversibility of the installation. These aspects have a critical relevance in the case of historical structures, whose features have to be preserved, and motivate researches about the use of FRCM on masonry structures, from both experimental and analytical points of view.

In this paper, the results of numerical analyses performed on arches unstrengthened and strengthened at the extrados with PBO-FRCM composites are presented, taking as reference the experimental tests published in [1] and [2]. The aim of this research is to further investigate the benefits that the use of FRCM composites have on the mechanical performance of masonry. The used model, implemented in the finite element code DIANA FEA, succeeded in reproducing the mechanical behavior of the considered arches in terms of collapse mechanism, load carrying capacity and ductility.

Peer-review under responsibility of the organizing committee of 10th ICM.

1 INTRODUCTION

Recent seismic events, which hit and heavily damaged large zones having a high density of masonry buildings, highlighted the high seismic vulnerability of arched structures if not appropriately retrofitted. Because of this, great attention is paid on the development of efficient repairing and strengthening solutions that can be applied on masonry arches in order to improve their structural capacity, both in terms of load carrying capacity and ductility.

In the last decades, composite materials such as Fiber Reinforcement Polymers (FRP) were widely used for this purpose, as they represent a valid alternative to traditional techniques. However, some criticisms have been recently made about the application of FRP composites on historical masonry buildings because of the following reasons:

- FRP composites are susceptible to degradation if exposed to high temperature,
- masonry structures strengthened with FRP collapse because of the delamination of the reinforcement system with significant loss of the substrate material at the bonded surface,
- the use of a polymeric matrix makes masonry impermeable to vapor,
- FRP composites cannot be applied on humid surfaces,
- the epoxy resins are in many cases chemically and physically incompatible with masonry,
- the intervention is not reversible.

These aspects have a critical relevance in the case of historical structures, whose features need to be preserved for conservation instances. Thus, the idea of substituting the organic matrix with an inorganic one, that is to use mortar instead of a resin as a matrix for the fibers, was proposed and developed for the creation of a new composite material called Fabric Reinforced Cementitious Matrix (FRCM).

A number of experimental studies regarding the effects of the application of FRCM composites on the mechanical behavior of masonry arches and vaults are available in the scientific literature (e.g. [3]-[7]), focusing on the comparison between the FRP and FRCM strengthening ([1],[2],[8],[9],[10]). The failure of masonry arches and vaults reinforced with FRCM composites is usually due to masonry crushing, detachment of the fibers at the fiber-matrix interface and/or of the reinforcement at the matrix-support interface, and to sliding along a masonry joint. The occurrence of one failure mode rather than another depends on different aspects, i.e. the application of the reinforcement to the extrados or intrados or both, the use of anchors to ensure the adherence between the strengthening system and the substrate, the presence of fill materials for masonry vaults.

In general, the failure of arches strengthened at the extrados is caused by the sliding of the arch along one joint and the detachment of the reinforcement at one of the abutments (e.g. [1],[2],[3],[9]). This failure mode is also associated to the damage of the matrix and the debonding at the fibers-matrix interface where the hinges opening is prevented by the presence of the reinforcement. In the scientific literature one example [5] has been found in which the use of steel anchor plates to fix the strengthening system at the supports prevented the detachment of the reinforcement and caused the rupture of the textile.

The failure mode of arches strengthened at the intrados is characterized by the detachment of the reinforcement at cross section where the load is applied (e.g. [6], [7]). The behavior of the reinforced arch can be influenced by the use of spike anchors or steel anchors, that hinder the reinforcement detachment in some points. The consequence is the fracture of the matrix and the rupture of the fibers in some cases, as it has been observed in the experimental campaign carried out in [3] or in [9], where the failure of the tested arches was due to laminate debonding. In particular, in [9], the fibers break between the fixed steel anchors where the

hinges open. For arches strengthened at both the extrados and the intrados the failure is caused by sliding along mortar joints. Consequently, the detachment of the reinforcement takes place at the extrados and intrados.

Different failure modes can be observed for reinforced vaults covered by fill materials, with the involvement of the adjacent structures, i.e. supports and spandrel walls (e.g. [8]).

It emerges from these studies that many aspects have to be taken in considerations when the failure modes of arches strengthened with FRCM composites are analyzed and that each case is different from the others, due to the geometrical features, that are of great importance for curved masonry structures, and to the interaction with adjacent structures. The scientific literature on the matter still needs to be enriched from an experimental and analytical point of view. [11]

Herein, the experimental data published in [1] and [2], regarding the reinforcement of two masonry arches with PBO-FRCM applied at the extrados and subjected to a vertical load applied at a quarter of the span, have been taken as reference to formulate a simplified micro-model with the purpose of investigating the improvement of the mechanical behavior of masonry arches reinforced at the extrados, in terms of load carrying capacity, kinematic and available kinematic ductility and failure mode. The finite element package DIANA FEA 10.1 [12] has been used to implement the model. The results of the performed numerical analyses are presented and fully commented.

2 UNSTRENGTHENED ARCH

The two unstrengthened arches (1-US and 2-US) tested in [2], whose geometrical features are reported in Table 1, were made using clay bricks and cement-lime mortar both produced by San Marco Laterizi Company. In particular, mix for the mortar was made using 1 part of Portland cement, 1 part of hydrated lime, two parts of water and 8 parts of sand. The load was applied under displacement control at a quarter of the span by means of a squared steel plate 20 mm thick and it was measured through a load cell with a capacity of 10 kN (TCLP-10B tension/compression load cell).

Centre	Internal radius	External radius	Thickness	Width	Span
(0,-433.5)	866	961	95	95	1500

Table 1: Geometrical features of the unstrengthened arch. Units: mm.

The unstrengthened masonry arch was modeled as a series of linear elastic isotropic blocks connected by non-linear interfaces, named BB (Block-Block), to simulate the presence of the mortar joints. The interaction between the blocks and the supports has been represented by an interface as well, labeled BS. The loading plate was also modeled, with reference to Figure 1, considering S235 steel. The mechanical characteristics of the blocks are listed in Table 2.

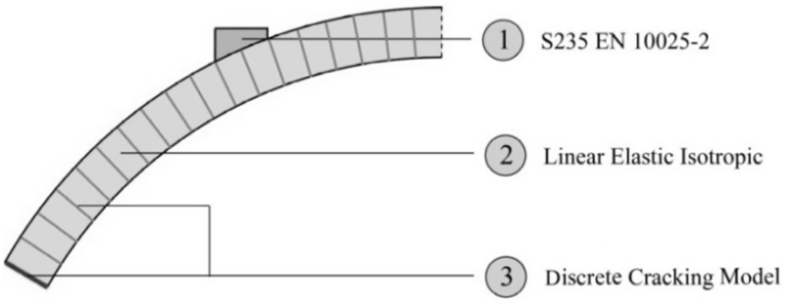

Figure 1: Micro-model materials scheme.

Young's modulus	Poisson's ratio	Mass density
MPa	-	T/mm^3
2700	0.2	$1.8e^{-9}$

Table 2: Mechanical characteristics of the elastic blocks.

The Discrete Cracking model [13] was used for the BB and BS interfaces. In particular, the normal and tangent stiffness were calibrated so that the initial stiffness of the arch could be comparable to that of the arches tested in [1]. The shear stiffness K_s was been put equal to the normal one K_n to avoid the sliding of the blocks along the mortar joints. The reduced shear modulus after cracking, K_s^*, was set equal to the 80% of K_s. The tensile strength was assumed to be equal to the value provided in [2], while for the tensile fracture energy a value low enough to reproduce the interface brittle behavior under traction was considered. These values are listed in Table 3.

K_n	K_s	f_t	G_t^I	K_s^*
N/mm^3	N/mm^3	MPa	N/mm	N/mm^3
1000	1000	0.3	0.01	800

Table 3: Mechanical parameters of the BB and BS interfaces.

For the numerical model 2D plane stress elements were used. In particular, for the plate and the blocks eight-node quadrilateral isoparametric plane stress elements, labeled CQ16M have been considered, while for the interfaces six-nodes interface elements (labeled CL12I) have been used. The elements size has been determined by diving the thickness in 9 parts of about 10.5x10.5 mm^2.

2.1 Numerical results

A non-linear analysis has been performed under displacement control and provided the load-displacement curve N-US displayed in Figure 2. The N-US curve is compared with the those of the arches tested in [1], labeled 1-US and 2-US. It can be noticed that for 1-US and 2-US arch, after the formation of the first hinge at 400 N and 550 N, revealed by a drop of load of about 50 N, the initial stiffness, equal to 6140 N/mm, is recovered. In particular, for 1-US arch, the stiffness recovery is delayed; in fact, the first drop of load is followed by a branch of the curve characterized by a reduced stiffness of about 2750 N/mm.

The curve corresponding to the numerical results fits the range of values defined by the two experimental curves; therefore, the initial stiffness K_1, equal to 4144 N/mm, is lower than the experimental ones.

The behavior of N-US arch is linear up to load of 565 N, which corresponds to the formation of the first hinge, and it is comparable with the ones of the arches 1-US and 2-US.

After the peak-load is reached at 991 N, the load decreases and a small softening branch is displayed with a slope equal to -5285 N/mm very similar to the ones determined for 1-US (-7378 N/mm) and 2-US (-5170 N/mm).

The softening branch is then followed an increasing deformation at almost constant load, similar to a plateau. Some sort of dissipation phenomenon seems to be occurring before the third hinge opens on the extrados at a symmetric position with respect to the load application point. This phenomenon is not recorded in the experimental tests taken as reference but it is similar to that obtained in [14], where a micro-model was formulated and calibrated on the

base of the same experimental data provided in [1] and [2].

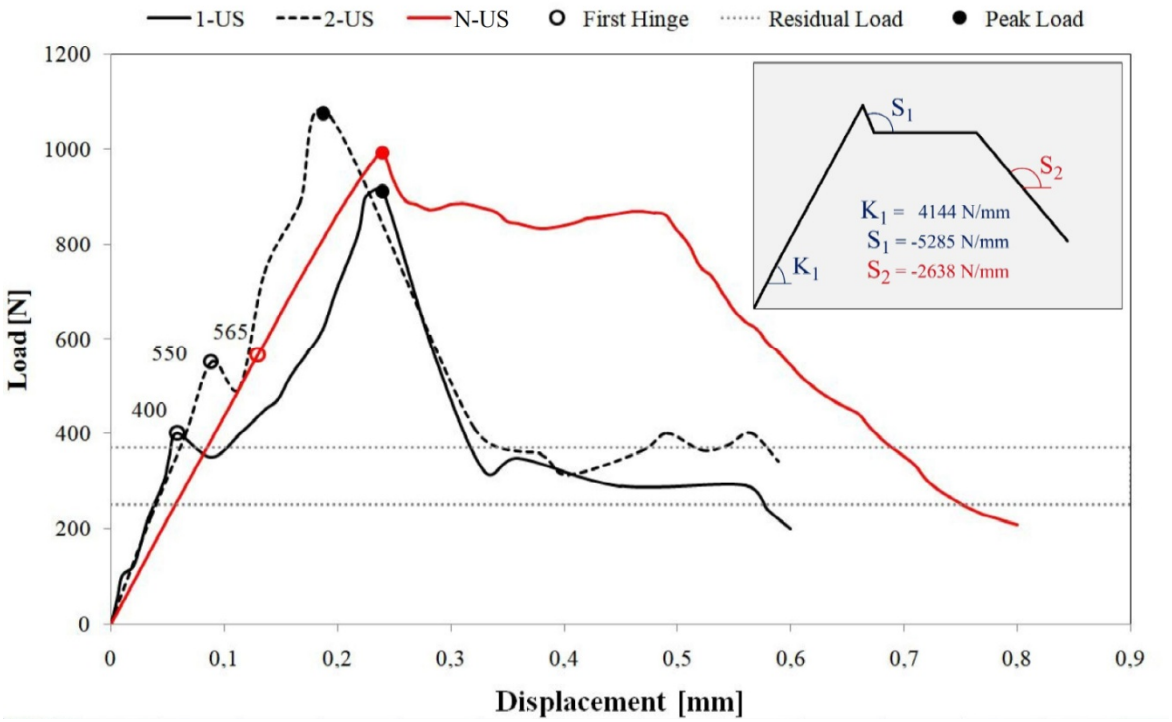

Figure 2: Load-displacement curves of the unstrengthened arches.

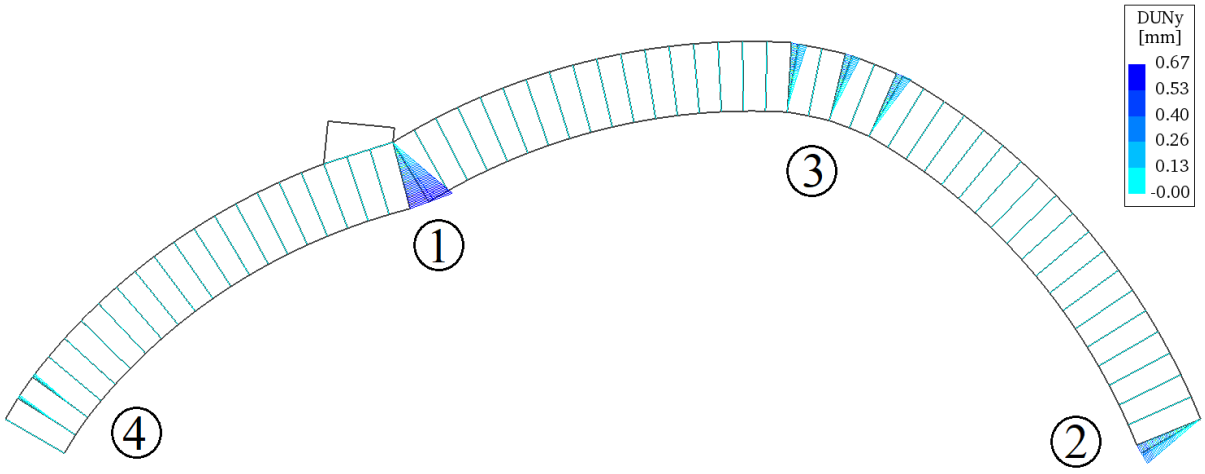

Figure 3: Interface relative displacements at the residual load.

After the opening of the third hinge, the load decreases following a softening law similar to the one of 1-US and 2-US up to a residual load equal to 207 N. In Figure 3 the interface relative displacements normal to the interface plane are displayed and the sequence according to which the hinges have formed is reported.

3 STRENGTHENED ARCHES

Two of the masonry arches tested in [2], labeled 1-PeS and 2-PeS, were reinforced at the extrados with a double layer (3+3 mm) of cementitious matrix characterized by an elastic modulus equal to 2874 MPa, a compressive strength of 20.22 Mpa and a flexural tensile

strength equal to 6.15 MPa. The textile (Ruredil Mesh gold) was made of PBO strips of 3 mm positioned at 11 mm one from each other to form a grid mesh, characterized by the properties listed in Table 4.

Weight of PBO fibers in the mesh	88	g/m^3
Equivalent dry fabric thickness in the direction of the warp	0.0455	mm
Equivalent dry fabric thickness in the direction of the weft	0.0115	mm
PBO Young's Modulus	223382	MPa
Tensile strength per unit width	46.59	N/mm

Table 4: Mesh properties.

In the following paragraphs the mechanical behavior of the arches strengthened at the extrados is analyzed and the features of the numerical model are reported.

3.1 Reference experimental results

In Figure 4 the load-displacement curves of 1-PeS and 1-PeS arches are shown. They are characterized by a similar behavior and same initial stiffness (9711.7 N/mm), which is sensibly higher than the one of 1-US and 2-US arches (6140 N/mm). Compared to other experimental tests available in literature (e.g.: [15], [16]), it is an uncommon case. In fact, the application of FRCM composites does not change the initial stiffness of the unstrengthened arches. From a numerical point of view, the aforementioned difference in the initial stiffness, observed in [1], would imply a change in the mechanical properties of the unstrengthened model, in particular in the BB interface stiffness. However, this choice is meaningless in this case because the aim of this study is not to perfectly fit some experimental results but to implement a numerical model able to reproduce the effect the considered strengthening system has on a masonry arch, in terms of ductility and load-carrying capacity.

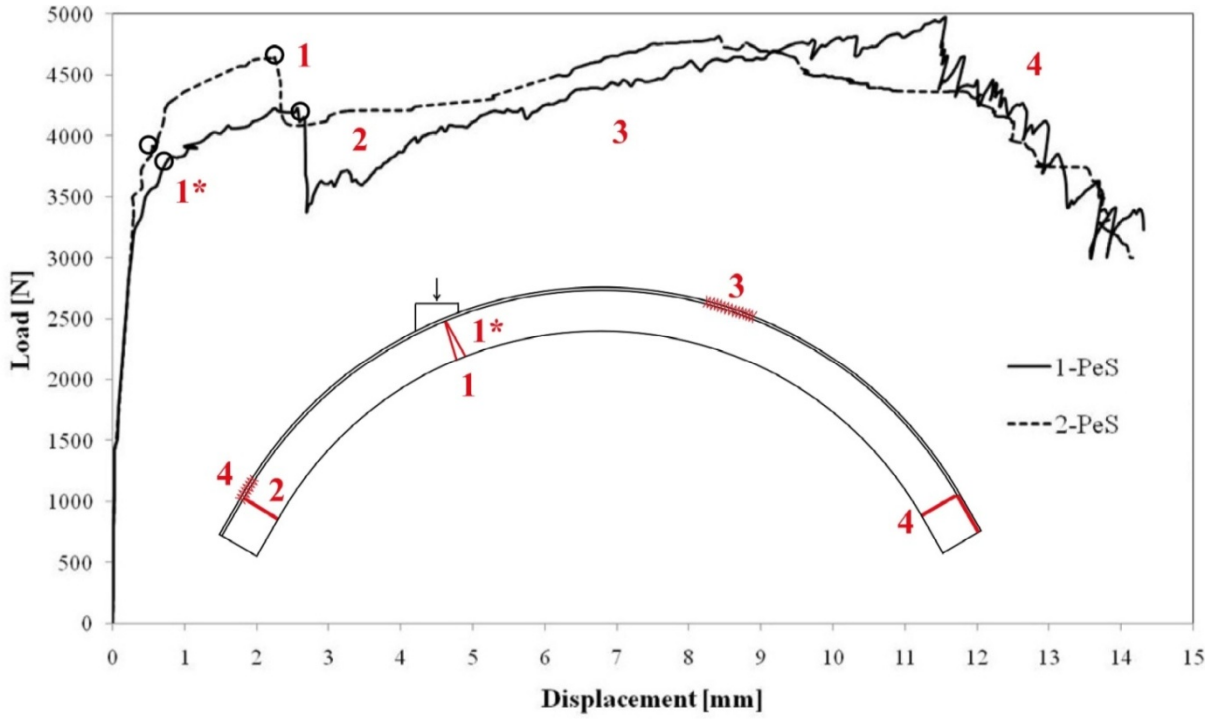

Figure 4: Hinges formation sequence for the PeS arches.

According to what is reported in [1], the onset of the first hinge under the loading plate corresponds to a load of 3780 N for the 1-PeS and 3825 N for the 2-PeS, which marks the limit of the linear elastic phase. In Figure 4 these points are marked with a circle and labeled 1*. The opening of the first hinge, named 1 in Figure 4, occurs at a load of 4222 N for the 1-PeS and 4639 N for the 2-PeS, followed by a sudden loss of load. A crack occurred on the mortar joint at the left abutment where the reinforcement prevented the opening of another hinge. Subsequently, the load increases very slowly up to the maximum load, that is 4968 N for 1-PeS and 4813 N for 2-PeS. During this phase, named 3 in Figure 4, the formation of small cracks on the surface of the cementitious matrix was observed. Finally, the shear sliding at the right abutment caused the collapse of the arches and the detachment of the reinforcement at the right abutment at the composite-support interface (point 4).

3.2 Features of the numerical model

The arch strengthened at the extrados was modeled on the base of the micro-model reported in section 2. The arch was covered by a double layer of cementitious matrix, as shown in Figure 5, with a thickness of 3+3 mm.

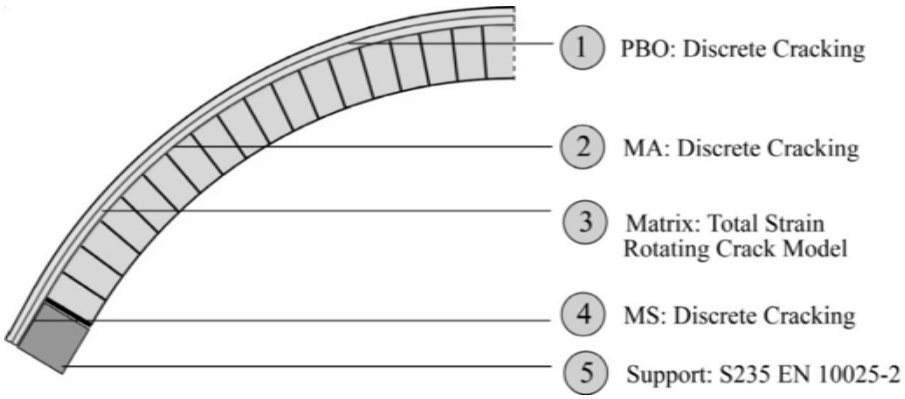

Figure 5: Modeling strategy.

Between the mortar layers a non-linear interface was put to reproduce the presence of the PBO fibers inside the matrix. The connection between the arch and the reinforcement system was also controlled by means of an interface, labeled MA. As the collapse of the strengthened arch was mainly due to the detachment of the strengthening system from the support of the arch, a non-linear interface, named MS, has been considered between the matrix and the support. The mechanical characteristics of MS and MA have been distinguished and listed in Table 6. The same type of constitutive model, i.e. the Discrete Cracking model, has been used for the PBO, MS and MA interfaces.

Total Strain Rotating Crack model [17] was used to reproduce the mechanical behavior of the cementitious matrix. In particular, the Young's modulus was provided by [1]; the Poisson's ratio was assumed to be equal to 0.2 and the mass density value was taken from the technical specifications of San Marco Laterizi company.

The value of the tensile strength is assumed to be lower than the flexural tensile strength provided in [2]. The softening behavior of the mortar under tension is governed by the JSCE stiffening model [18], which is characterized by the presence of a small plateau before the softening branch. The compressive strength was set equal to the value provided by the experimental tests taken as reference for this study, while the compressive fracture energy was determined using the formula given by the Model Code 90 for values of compressive strength ranging between 12 and 80 MPa.

Young's modulus	Poisson's ratio	Mass density	Tensile strength	Plateau and strain	Compressive strength	Compressive fracture energy
E	ν	ρ	f_t	ε_{tu}	f_c	G_c
MPa	-	T/mm^3	MPa	-	MPa	N/mm
2874	0.2	1.8e^{-9}	4	0.002	20	22.16

Table 5: Mechanical characteristics of the cementitious matrix.

The calibration of the mechanical parameters of the MA, MS and PBO interfaces has been done on the base of the following considerations:

- the tensile strength of the MS interfaces should not be very different from the BS interface tensile strength,
- the tensile fracture energy of the interfaces should be low enough to determine the sudden crack of the material,
- the tensile strength of the MA interface should be lower than the one of the matrix,
- the tensile strength of the PBO interface should be higher than the one of the matrix,
- the shear modulus after cracking of MS, MA and the PBO should be very low in order to let the relative sliding between the arch and the reinforcement and between the fibers and the matrix, after the formation of cracks in the matrix. [11]

	K_n	K_s	f_t	G_t^I	K_s^*
	N/mm^3	N/mm^3	MPa	N/mm	N/mm^3
MS	500	500	0.35	0.1	5
MA	500	500	2	0.5	5
PBO	500	500	5	0.5	10

Table 6: Mechanical characteristic of the "Matrix-Support" (MS), "Matrix-Arch" (MA) and "PBO" interface.

In Figure 6 the load-displacement curve of the strengthened arch (ExS) is plotted and compared with the experimental curves (1-PeS and 2-PeS) and the numerical results obtained for the unstrengthened arch, N-US. The initial stiffness of the ExS arch is the same as the N-US arch up to a value of 1039 N, which corresponds to the opening of the first hinge under the loading plate. As a consequence, the global stiffness of the arch is reduced from a value of 4144 N/mm to 1232 N/mm (K_3 in Figure 8), that is comparable with the reduced stiffness values of 1-PeS and 2-PeS arches, i.e. K_1 = 1037 N/mm and K_2 = 1549 N/mm respectively. A detail of the arch is reported in Figure 6, showing the opening of the first hinge and the linear diagram of the relative interface displacements, normal to the interface itself. At a load of 2617 N a sudden loss of load of about 170 N is recorded, due to the sliding of the blocks along the mortar joint at the right abutment (see the detail in Figure 6).

After this point the load increases until some cracks appear in the mortar at the left abutment, where the presence of the reinforcement hindered the BB interfaces opening. As the load increases, more cracks appear; the arch stiffness is reduced to a value of 345 N/mm and the curve almost fits the one corresponding to 1-PeS. Then, at a load of about 4100 N, large displacements occur at almost constant load and the formation of numerous cracks is observed in the matrix at a symmetric position with respect to the loading plate. The detachment of the

reinforcement at the right abutment progresses causing the collapse of the arch with the load slightly decreasing up to 3912 N (Table 7).

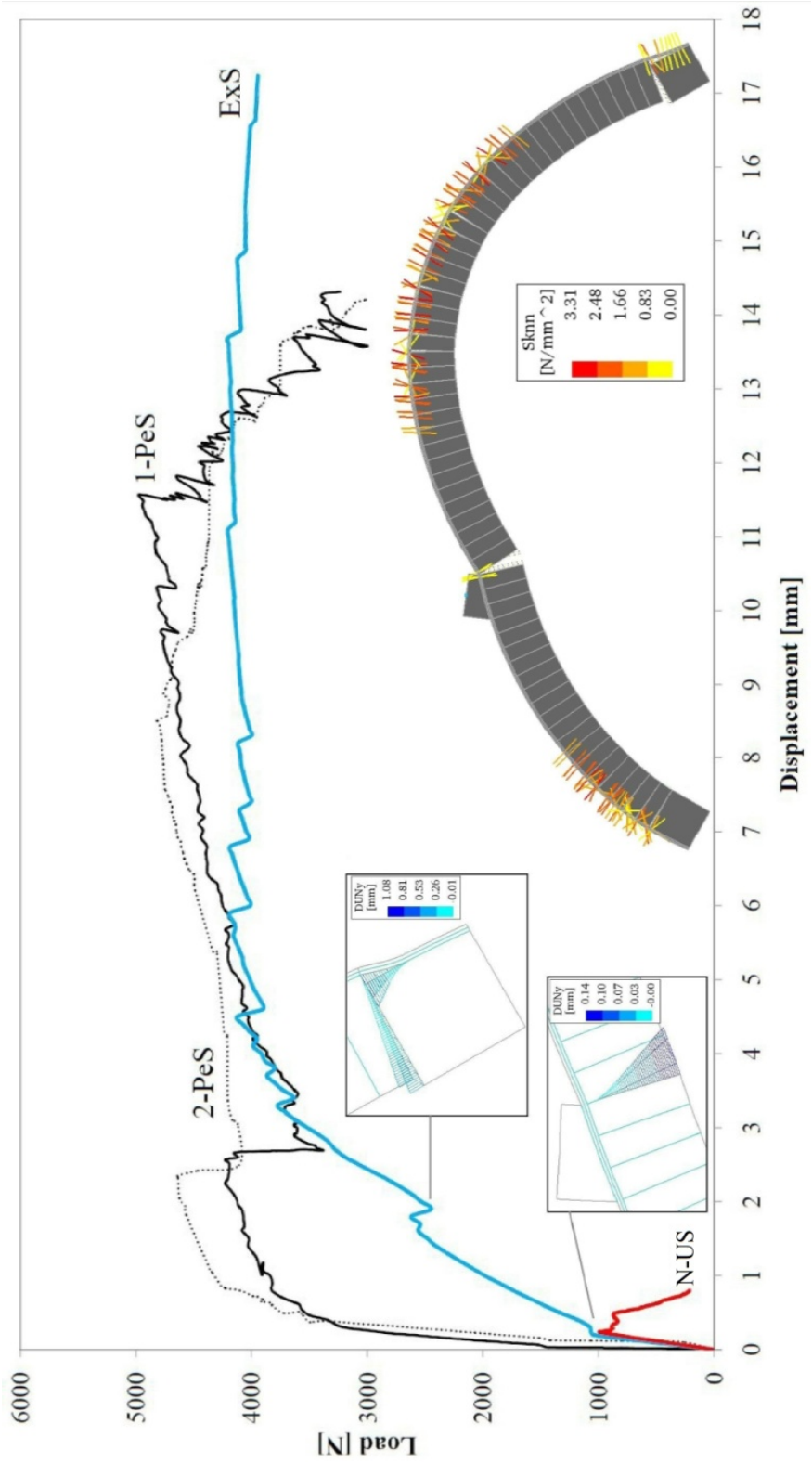

Figure 6: Numerical and experimental load-displacement curves of the unstrengthened and strengthened arches. Deformed configuration of the arch at the last converged step.

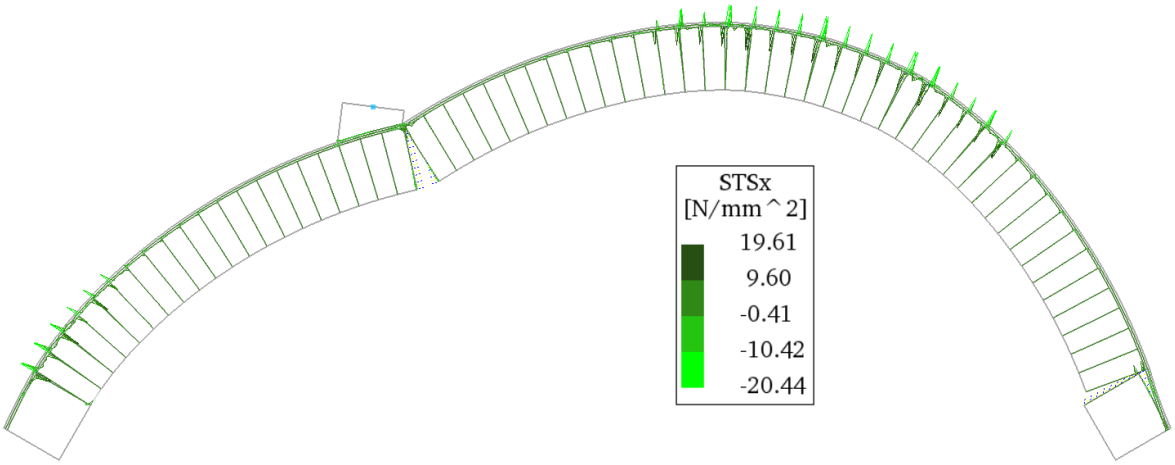

Figure 7: Interface tractions along x local axis.

The collapse mechanism was correctly reproduced. In Figure 6 the deformed configuration of the arch at collapse is reported with the corresponding cracks. If it is compared with Figure 7, where the linear diagrams of the shear interface tractions are displayed, it is evident that the formation of cracks in the mortar is associated to the sliding at the MA interface where the opening of hinges was hindered by the presence of the reinforcement. The limit strength of the PBO is never reached, as it is also confirmed by the reference experimental data [2].

The load carrying capacity of the modeled arch is comparable to that of the tested ones. The peak load is equal to 4185 N, which is not very different from the values reached by 1-PeS and 2-PeS arches (see

Table 7).

	Limit of the elastic phase	x_e	Peak load	x_m	80% of the peak load	x_u	μ_k	μ_{ak}
	N	mm	N	mm	N	mm	mm/mm	mm/mm
1-PeS	3223	0.3	4968	11.57	3974	12.67	38.56	1.95
2-PeS	3490	0.37	4813	8.51	3850	12.9	23	1.516
ExS	1039	0.2	4185	5.9	3912	17.3	29.5	2.93
1-US	400	0.059	910	0.24	728	0.264	4.068	1.1
2-US	550	0.089	1066	0.19	853	0.235	2.13	1.23
N-US	565	0.13	991	0.24	793	0.51	1.85	2.125

Table 7: Characteristic points for the determination of the kinematic and available kinematic ductility. Comparison between the experimental and numerical resuls.

The kinematic ductility, μ_k, of the ExS arch was determined as the ratio of the displacement at the maximum load, x_m, to the displacement measured at the end of the linear elastic phase, x_e. In Figure 8 the load-displacement curves of the strengthened arches are schematized and the characteristic points of the load-displacement curves 1/2-PeS and ExS are marked, with the subscripts "1", "2" and "3" referring to 1-PeS, 2-PeS and ExS, respectively. For ExS a value of μ_k equal to 29.5 mm/mm is obtained, practically the same of the kinematic ductility mean value determined for 1/2-PeS arches (30.78 mm/mm). Therefore, the increment of kinematic ductility from the unstrengthened arch N-US to the strengthened one ExS is almost

the same of that provided in [1].

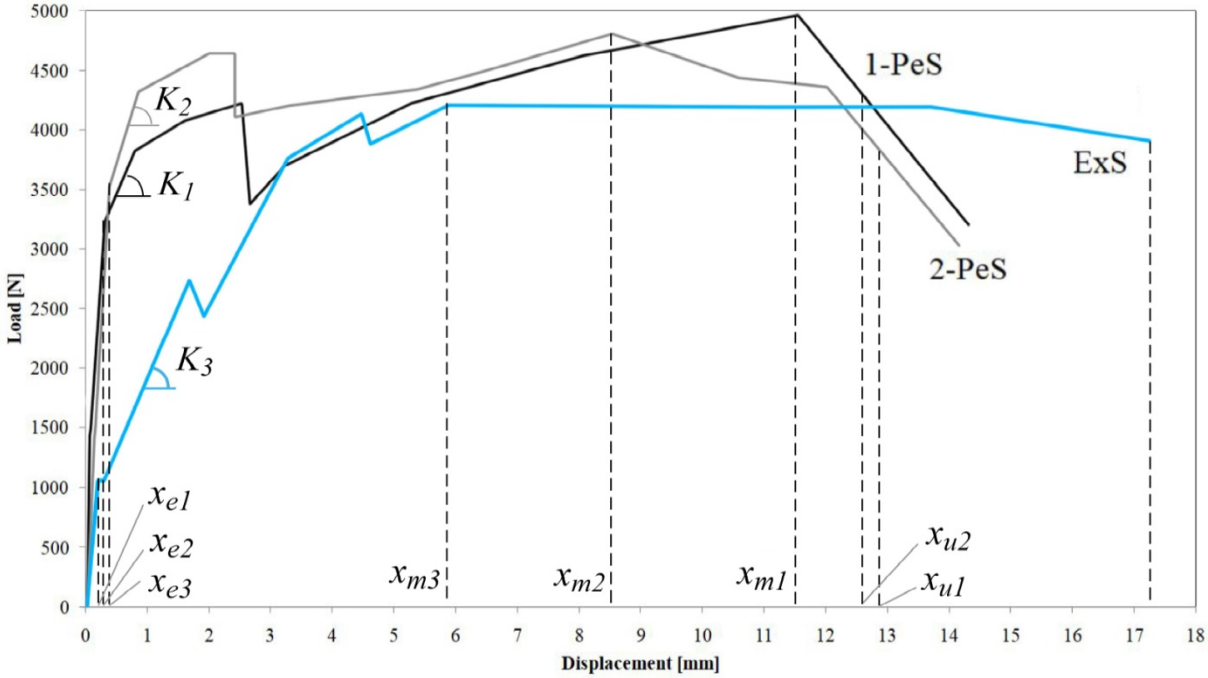

Figure 8: Characteristic points for the kinematic and available kinematic ductility determination.

The available kinematic ductility, μ_{ak}, i.e. the capacity of the specimen to show large displacements after the maximum load up to the ultimate load, conventionally considered equal to the 80% of the maximum load, has been determined as the ratio of x_u, the displacement corresponding to the ultimate load, to x_m. A value of 2.93 mm/mm is obtained, higher than the experimental ones. Nevertheless, the ratio $\mu_{ak}(ExS)/\mu_{ak}(MiM)=1.37$ is comparable to the one obtained considering the mean values of the PeS and US arches, $\mu_{ak}(ExS)/\mu_{ak}(MiM)=1.487$.

On the base of the reported considerations, it can be stated that the implemented model is reliable and effective in reproducing the collapse mechanism of the reinforced arches tested in [1][2] and their load carrying capacity in terms of peak-load and ductility.

4 CONCLUSIONS

- The mechanical behavior of the arch reinforced at the extrados with PBO-FRCM composites was analyzed using a simplified micro-model approach, formulated on the base of the experimental data published in [1] and [2], implemented with the Finite Element package DIANA 10.1 and calibrated referring to the results obtained for the unstrengthened arches.
- The initial stiffness of the numerically modeled arch ExS is different from the one of the arches tested in [1]. The initial stiffness of 1/2-PeS arches is uncommonly different from that of the unstrengthened arches, if compared to other cases available in the scientific literature. In order to fit the experimental tests, the mechanical parameters defining the arch in the micro-model should be changed, but no reasons were given in the reference paper to justify this difference of initial stiffness. Therefore, it was considered appropriate to keep the mechanical parameters of the micro-model unchanged.

- In the numerical model, the first hinge opens at a load of 1039 N while, according to what is reported in [1], the first hinge occurs at 3780 N for the 1-PeS arch and 3825 N for the 2-PeS arch. Nevertheless, the reduced stiffness, after the opening of the first hinge, for the three arches are comparable.
- The values of kinematic and available kinematic ductility obtained from the numerical model were very similar to those determined on the base of the experimental data. Moreover, the same increment of ductility was provided by the application of the reinforcement both for the experimental and numerical arches, with reference to the unstrengthened ones.
- The collapse mechanism of the strengthened arch was correctly reproduced.

REFERENCES

[1] V. Alecci, F. Focacci, L. Rovero, G. Stipo, M. De Stefano, Extrados strengthening of brick masonry arches with PBO–FRCM composites: Experimental and analytical investigations. *Composite Structures*, **149**, 184-196, 2016.

[2] V. Alecci, G. Misseri, L. Rovero, L. Feo, R. Luciano, Experimental investigation on masonry arches strengthened with PBO-FRCM composite. *Composites Part B*, **100**, 228-239, 2016.

[3] L. Garmendia, P. Larrinaga, D. García, I. Marcos, Textile-reinforced mortar as strengthening material for masonry arches. *International Journal of Architectural Heritage*, **8**(5), 627-648, 2014.

[4] L. Garmendia, I. Marcos, E. Garbin, M. R. Valluzzi, Strengthening of masonry arches with Textile-Reinforced Mortar: experimental behaviour and analytical approaches. *Materials and Structures*, **47**(12), 2067-2080, 2014.

[5] Ł. Hojdys, P. Krajewsky, Laboratory tests on masonry vaults strengthened at the extrados. *Proc. 9th Int. Conf. on Structural Analysis of Historical Constructions*, R. Meli, F. Peña & M. Chávez eds.,2014.

[6] S. De Santis, F. Roscini, G. de Felice, Retrofitting masonry vaults with basalt Textile Reinforced Mortar. *Key Engineering Materials*, **747**, 250-257, 2017.

[7] N. H. Sadeghi, D. V. Oliveira, R. A. Silva, N. Mendes, M. Correia, H. Azizi-Bondarabadi, Performance of Adobe vaults strengthened with LC-TRM: an experimental approach. *Proc. 3th Int. Conf. on Protection of Historical Constructions*, F. M. Mazzolani, A. Lamas, L. Calado, J. M. Proença & B. Faggiano eds., IST Press, Lisbon, 2017.

[8] S. Briccoli Bati, L. Rovero, U. Tonietti, Strengthening masonry arches with composite materials. *Journal of composites for Construction*, **11**(1), 33-41, 2007.

[9] A. Borri, P. Casadei, G. Castori, J. Hammond, Strengthening of brick masonry arches with externally bonded steel reinforced composites. *Journal of composites for construction*, **13**(6), 468-475, 2009.

[10] F. G. Carozzi, C. Poggi, E. Bertolesi, G. Milani, Ancient masonry arches and vaults strengthened with TRM, SRG and FRP composites: Experimental evaluation. *Composite Structures*, **187**, 466-480, 2018.

[11] E. Ricci, *Numerical analysis of masonry arches: Limit Analisys and FE simulations.* PhD Thesis, University of Cassino and SL, University of Cassino, Cassino (IT), 2018.

[12] DIANA Finite Element Analysis User's Manual Release 10.1. Delft, The Netherlands, 2016.

[13] H. A. W. Cornelissen, D. A. Hordijk, H. W. Reinhardt, Experimental determination of crack softening characteristics of normalweight and lightweight concrete. *Heron*, **32**(2), 45-56, 1986.

[14] B. Pantò, M. Malena, G. de Felice, Non-linear modeling of masonry arches strengthened with FRCM. *Key Engineering Materials*, **747**, 93-100, 2017.

[15] L. Rovero, F. Focacci, G. Stipo, Structural behavior of arch models strengthened using fiber-reinforced polymer strips of different lengths. *Journal of Composites for Constructions*, **17**, 249-258, 2013.

[16] A. Baratta, O. Corbi, Stress analysis of masonry vaults and static efficacy of FRP repairs. *International Journal of Solids and Structures*, **44**(24), 8028–8056, 2007.

[17] J. G. Rots, *Computational Modeling of Concrete Fracture.* PhD Thesis, Delft University of Technology, Delft University Press, Delft (NL), 1988.

[18] JSCE Guidelines for Concrete No. 15: Standard Specifications for Concrete Structures - 2007 "Design". Tech. rep., Japan Society of Civil Engineers. 2010.